Stable Anisotropic Materials

Yijing Li, *Member, IEEE*, and Jernej Barbič, *Member, IEEE*

Abstract—The Finite Element Method (FEM) is commonly used to simulate isotropic deformable objects in computer graphics. Several applications (wood, plants, muscles) require modeling the directional dependence of the material elastic properties in three orthogonal directions. We investigate linear orthotropic materials, a special class of linear anisotropic materials where the shear stresses are decoupled from normal stresses, as well as general linear (non-orthotropic) anisotropic materials. Orthotropic materials generalize transversely isotropic materials, by exhibiting different stiffness in three orthogonal directions. Orthotropic materials are, however, parameterized by nine values that are difficult to tune in practice, as poorly adjusted settings easily lead to simulation instabilities. We present a user-friendly approach to setting these parameters that is guaranteed to be stable. Our approach is intuitive as it extends the familiar intuition known from isotropic materials. Similarly to linear orthotropic materials, we also derive a stability condition for a subset of general linear anisotropic materials, and give intuitive approaches to tuning them. In order to simulate large deformations, we augment linear corotational FEM simulations with our orthotropic and general anisotropic materials.

Index Terms—Computer graphics, animation, orthotropic materials, anisotropic materials, finite element method

1 Introduction

Simulation of three-dimensional solid deformable models is important in many applications in computer graphics, robotics, special effects and virtual reality. Most applications in these fields have been limited to isotropic materials, i.e., materials that are equally elastic in all directions. Many real materials are, however, stiffer in some directions than others. The space of such anisotropic materials is vast and not easy to navigate, tune or control. In this paper, we first study linear *orthotropic* materials, and then extend them to general linear anisotropic materials. Orthotropic materials exhibit different stiffnesses in three orthogonal directions (called material directions, not to be confused with the principal directions as obtained through an SVD of the deformation gradient); formally, they possess three orthogonal planes of rotational symmetry. As a real-world example of an orthotropic material, consider wood, which exhibits different material properties along the axial, radial and circumferential directions of a tree branch. In the coordinate system of the material directions, orthotropic materials have the special property that normal stresses only cause normal strains, and shear stresses only cause shear strains, a property which is not valid for general anisotropic materials. Orthotropic materials form an intuitive subset of all anisotropic materials, as they generalize the familiar isotropic, and transversely isotropic, materials to materials with three different stiffness values in some three orthogonal directions. Although simpler than fully general anisotropic materials, orthotropic materials still require tuning nine independent parameter values. In practice, this task is difficult due to the large number of parameters and because many of the settings lead to unstable simulations in a non-obvious way. In this paper, we study orthotropic materials from the point of view of practical simulation in computer graphics and related fields. We demonstrate how to intuitively and stably tune orthotropic material parameters, by parameterizing the six Poisson's ratios using a stable one-dimensional parameter family, similar to the intuition from isotropic simulation. Once we derive stability conditions for linear orthotropic simulations, we then extend them to a subset of general linear (non-orthotropic) anisotropic materials, making it possible to model linear anisotropic materials that shear sideways in a prescribed direction when subjected to a normal load. We derive a necessary and sufficient condition for such general linear anisotropic materials and demonstrate how they can be intuitively tuned. Our work makes it possible to easily augment existing simulation solvers with stable and intuitive anisotropic effects. We limit the discussion to linear materials which have a linear relationship between stress and strain. We support large deformations by using the linear corotational FEM simulation [1].

2 Related Work

Anisotropic materials are discussed in many references, see, e.g. [2]. Transversely isotropic hyperelastic materials were presented by Bonet and Burton [3]. Picinbono et al. [4] proposed a non-linear FEM model to simulate soft tissues with large deformations and transversely isotropic behavior. Thije et al. [5] addressed the instabilities that occur under strong anisotropy, and provided a simple updated Lagrangian FEM scheme to handle the problem. Zhong et al. [6] simulated isotropic and anisotropic materials by the reaction-diffusion analogy, and Kharevych et al. [7] established a method to coarsen heterogeneous isotropic materials into anisotropic materials. For medical simulation, Picinbono et al. [8] described a surgery simulator that can model linear transversely isotropic materials at haptic rates and also presented a nonlinear transversely isotropic model [9]. Liao et al. [10]

• *The authors are with the Department of Computer Science, University of Southern California, Los Angeles, CA 90089. E-mail: {yijingl, jnb}@usc.edu.*

Manuscript received 25 Oct. 2014; revised 13 May 2015; accepted 9 June 2015. Date of publication 21 June 2015; date of current version 4 Sept. 2015. Recommended for acceptance by E. Sifakis and V. Koltun.
For information on obtaining reprints of this article, please send e-mail to: reprints@ieee.org, and reference the Digital Object Identifier below.
Digital Object Identifier no. 10.1109/TVCG.2015.2448105

generated transversely isotropic and orthotropic bone materials from CT data, whereas Sagar et al. [11] used an orthotropic material for modeling the cornea. Sermesant [12], [13] and Talbot et al. [14] adopted a transversely isotropic material in constructing an electro-mechanical model of the heart. Comas et al. [15] implemented a transversely isotropic visco-hyperelastic model on the GPU, and Teran et al. [16], Sifakis [17], [18] and Zhou and Lu [19] simulated human muscles with a transversely isotropic, quasi-incompressible model. Irving et al. [20] proposed a robust, large-deformation invertible simulation method and demonstrated it with transversely isotropic models. There are other methods to achieve anisotropic behaviors. Liu et al. [21] used composite materials to enable anisotropic behaviors, Martin et al. [22] achieved anisotropic results by guiding objects towards certain predefined shapes, and Hernandez et al. [23] imposed anisotropic strain-limiting constraints.

Cloth materials often exhibit anisotropic behaviors because of their fiber components [24]. Etzmuß et al. [25] used an orthotropic Finite Element cloth model, Huber et al. [26] introduced wet cloth with orthotropic material models and Garg et al. [27] developed an orthotropic material using a hinge-based bending model. Peng and Cao[28] developed a non-orthotropic constitutive model to characterize the anisotropic cloth behavior. Thomaszewski [29] imposed limits on the individual entries of the Cauchy strain tensor to simulate anisotropic, bi-phasic textile materials. Wang et al. [30] proposed a piecewise linear anisotropic cloth material model and Allard et al. [31] used a 2D anisotropic material to simulate thin soft tissue tearing.

Previous anisotropic solid simulations in computer graphics mostly focused on transversely isotropic materials where two directions have equal stiffness, leading to five tunable parameters. We generalize linear materials to linear orthotropic materials with three distinct stiffnesses in three orthogonal directions, and present an intuitive approach to tune the resulting nine parameters. To the best of our knowledge, we are first work in computer graphics to analyze solid linear orthotropic materials and general linear anisotropic materials in substantial detail. Previous papers on orthotropic and general anisotropic solid materials in engineering assumed that the nine orthotropic or 21 general anisotropic parameters are given or measured from real materials [32], [33]. In contrast, we provide an intuitive way for the users to tune them and ensure they are stable.

Our work uses corotational linear FEM materials introduced in [1]. Construction of the stiffness matrix for linear FEM materials can also be found, for example, in [34].

3 Orthotropic Materials

We now introduce linear orthotropic materials. Given the deformation gradient F, the Green-Lagrange strain is defined as $\epsilon^{3\times3} = (F^T F - I)/2$, and the Cauchy stress $\sigma^{3\times3}$ gives the elastic forces per surface area in a unit direction n, as $\sigma^{3\times3} n$ [34]. Note that we can operate with Cauchy stresses here as they are equivalent to other forms of stresses (Piola) due to the small-deformation analysis; we achieve large deformations via corotational linear FEM [1]. The 6×6 elasticity tensor $\mathcal{S}$ relates strain ϵ to stress σ via $\epsilon = \mathcal{S}\sigma$, where we have unrolled the 3×3 symmetric matrices $\epsilon^{3\times3} = [\epsilon_{ij}]_{ij}$ and $\sigma^{3\times3} = [\sigma_{ij}]_{ij}$ into 6-vectors, using the 12, 23, 31 ordering of the shear components as in [34]:

$$\epsilon = [\epsilon_{11}\ \epsilon_{22}\ \epsilon_{33}\ 2\epsilon_{12}\ 2\epsilon_{23}\ 2\epsilon_{31}]^T, \tag{1}$$

$$\sigma = [\sigma_{11}\ \sigma_{22}\ \sigma_{33}\ \sigma_{12}\ \sigma_{23}\ \sigma_{31}]^T. \tag{2}$$

Components $11, 22, 33$ are called normal components, whereas $12, 23, 31$ are referred to as shear components. The inverse elasticity tensor $\mathcal{C} = \mathcal{S}^{-1}$ relates σ to ϵ, via $\sigma = \mathcal{C}\epsilon$. The elasticity tensor must be symmetric and therefore it has 21 independent entries for a general anisotropic material,

$$\mathcal{C} = \begin{bmatrix} \mathcal{C}_{11} & \mathcal{C}_{12} & \mathcal{C}_{13} & \mathcal{C}_{14} & \mathcal{C}_{15} & \mathcal{C}_{16} \\ & \mathcal{C}_{22} & \mathcal{C}_{23} & \mathcal{C}_{24} & \mathcal{C}_{25} & \mathcal{C}_{26} \\ & & \mathcal{C}_{33} & \mathcal{C}_{34} & \mathcal{C}_{35} & \mathcal{C}_{36} \\ & & & \mathcal{C}_{44} & \mathcal{C}_{45} & \mathcal{C}_{46} \\ & Sym. & & & \mathcal{C}_{55} & \mathcal{C}_{56} \\ & & & & & \mathcal{C}_{66} \end{bmatrix}. \tag{3}$$

Once $\mathcal{C}$ is known, the stiffness matrix for a linear tetrahedral element is computed as $K^e = V^e B^{eT} \mathcal{C}^e B^e$, where V^e is the volume of tet e, and B^e is a 6×12 strain-displacement matrix determined by the initial shape of tet e (see [34] or [1]),

$$B^e = [\, B_0 \quad B_1 \quad B_2 \quad B_3 \,], \tag{4}$$

where we have dropped index e for simplicity and

$$B_i = \begin{bmatrix} a_i & 0 & 0 & b_i & 0 & c_i \\ 0 & b_i & 0 & a_i & c_i & 0 \\ 0 & 0 & c_i & 0 & b_i & a_i \end{bmatrix}^T. \tag{5}$$

Here, a_i, b_i, c_i are computed as follows:

$$\begin{bmatrix} * & a_0 & b_0 & c_0 \\ * & a_1 & b_1 & c_1 \\ * & a_2 & b_2 & c_2 \\ * & a_3 & b_3 & c_3 \end{bmatrix} = \begin{bmatrix} 1 & 1 & 1 & 1 \\ x_0 & x_1 & x_2 & x_3 \\ y_0 & y_1 & y_2 & y_3 \\ z_0 & z_1 & z_2 & z_3 \end{bmatrix}^{-1}, \tag{6}$$

where (x_i, y_i, z_i), $i = 0, 1, 2, 3$ are the vertices of tet e in the undeformed configuration.

Unlike isotropic materials that are parameterized by a single Young's modulus and Poisson's ratio, orthotropic materials have three different Young's moduli E_1, E_2, E_3, one for each orthogonal direction, and six Poisson's ratios ν_{ij}, for $i \neq j$, only three of which are independent. Young's modulus E_i gives the stiffness of the material when loaded in orthogonal direction i. Poisson's ratio ν_{ij} gives the contraction in direction j when the extension is applied in direction i. In a general anisotropic material, both the normal and shear components of strain affect both the normal and shear components of stress, i.e., matrix $\mathcal{C}$ is dense. In orthotropic materials, however, the normal and shear components are decoupled: normal stresses only cause normal strains, and shear stresses only cause shear strains. Furthermore, individual shear stresses in the $12, 23, 31$ planes are decoupled from each other: strain ϵ_{ij} $(i \neq j)$ only depends on stress σ_{ij} via a scalar parameter (shear modulus) μ_{ij}. Under these assumptions, the elasticity tensor has 9 free parameters and takes a block-diagonal form. It is easiest to first state its inverse

$$\mathcal{S}_{ortho} = \begin{bmatrix} \frac{1}{E_1} & -\frac{\nu_{21}}{E_2} & -\frac{\nu_{31}}{E_3} & 0 & 0 & 0 \\ -\frac{\nu_{12}}{E_1} & \frac{1}{E_2} & -\frac{\nu_{32}}{E_3} & 0 & 0 & 0 \\ -\frac{\nu_{13}}{E_1} & -\frac{\nu_{23}}{E_2} & \frac{1}{E_3} & 0 & 0 & 0 \\ 0 & 0 & 0 & \frac{1}{\mu_{12}} & 0 & 0 \\ 0 & 0 & 0 & 0 & \frac{1}{\mu_{23}} & 0 \\ 0 & 0 & 0 & 0 & 0 & \frac{1}{\mu_{31}} \end{bmatrix}. \quad (7)$$

The orthotropic elasticity tensor is then

$$\mathcal{C}_{ortho} = \mathcal{S}_{ortho}^{-1} = \begin{bmatrix} A & 0 \\ 0 & B \end{bmatrix}, \quad \text{for} \quad (8)$$

$$A = \Upsilon \begin{bmatrix} E_1(1-\nu_{23}\nu_{32}) & E_2(\nu_{12}+\nu_{32}\nu_{13}) & E_3(\nu_{13}+\nu_{12}\nu_{23}) \\ E_1(\nu_{21}+\nu_{31}\nu_{23}) & E_2(1-\nu_{13}\nu_{31}) & E_3(\nu_{23}+\nu_{21}\nu_{13}) \\ E_1(\nu_{31}+\nu_{21}\nu_{32}) & E_2(\nu_{32}+\nu_{12}\nu_{31}) & E_3(1-\nu_{12}\nu_{21}) \end{bmatrix}, \quad (9)$$

$$B = \begin{bmatrix} \mu_{12} & 0 & 0 \\ 0 & \mu_{23} & 0 \\ 0 & 0 & \mu_{31} \end{bmatrix}, \quad \text{and} \quad (10)$$

$$\Upsilon = \frac{1}{1-\nu_{12}\nu_{21}-\nu_{23}\nu_{32}-\nu_{31}\nu_{13}-2\nu_{21}\nu_{32}\nu_{13}}. \quad (11)$$

Equations (7) and (8) give elasticity tensors with respect to the world coordinate axes. A general linear orthotropic material, however, assumes the block-diagonal form given in Equations (7) and (8) only in a special orthogonal basis, given by the three material axes where the stiffnesses are E_1, E_2, E_3. In other bases (including world-coordinate axes), its form looks generic, as in Equation (3). Therefore, to model orthotropic materials whose material axes are not aligned with the world axes, we need to convert elasticity tensors from one basis to another. For a basis given by a rotation Q, the elasticity tensor $\mathcal{C}$ transforms as follows:

$$\mathcal{C}_{world} = K\mathcal{C}_{local}K^T, K = \begin{bmatrix} K^{(1)} & 2K^{(2)} \\ K^{(3)} & K^{(4)} \end{bmatrix}, \quad \text{for} \quad (12)$$

$$K^{(1)}_{i,j} = Q^2_{i,j}\,, \qquad K^{(2)}_{i,j} = Q_{i,j}Q_{i,(j+1)\bmod 3}, \quad (13)$$

$$K^{(3)}_{i,j} = Q_{i,j}Q_{(i+1)\bmod 3,j}, \quad (14)$$

$$K^{(4)}_{i,j} = Q_{i,j}Q_{(i+1)\bmod 3,(j+1)\bmod 3} + \quad (15)$$

$$+ Q_{i,(j+1)\bmod 3}Q_{(i+1)\bmod 3,j}. \quad (16)$$

The rotation matrix Q is an input parameter for constructing the orthotropic material, and can vary spatially on the model (our cylinder and fern examples). It can be made, for example, to correspond to the directional derivatives of a 3D uvw texture map.

3.1 Special Cases

When two of the three orthogonal directions are equally stiff, one obtains the *transversely isotropic* material. For such a material, there is a plane in which the material is isotropic, but the orthogonal direction is not. There are five free parameters, E_p, E_z and ν_p, ν_{pz} and μ_{zp}, and we have $E_1 = E_2 = E_p, E_3 = E_z, \nu_{12} = \nu_{21} = \nu_p, \nu_{13} = \nu_{23} = \nu_{pz}, \nu_{31} = \nu_{32} = \nu_{zp} = \nu_{pz}E_z/E_p, \mu_{12} = E_p/2(1+\nu_p), \mu_{23} = \mu_{31} = \mu_{zp}$. A further simplification is the isotropic material which has just two free parameters E and ν and we have $E_1 = E_2 = E_3 = E, \nu_{ij} = \nu$ for all i, j and $\mu_{12} = \mu_{23} = \mu_{31} = E/2(1+\nu)$.

4 Setting the Orthotropic Parameters

In order to keep the elasticity tensor symmetric, the Poisson's ratios have to satisfy

$$\frac{\nu_{ij}}{E_i} = \frac{\nu_{ji}}{E_j}, \quad (17)$$

for all $i \neq j$. Therefore, only three of the six Poisson's ratios are independent. This leaves a total of nine free parameters in the linear orthotropic material: E_1, E_2, E_3, $\nu_{12}, \nu_{23}, \nu_{31}, \mu_{12}, \mu_{23}, \mu_{31}$. There are stability limitations on these nine parameters. In order for the elastic strain energy to be a positive-definite function of ϵ, the elasticity tensor $\mathcal{C}_{ortho}$ must be positive-definite. Material is unstable if $\mathcal{C}_{ortho}$ is not positive-definite because then, there exists a strain direction that causes a negative stress, i.e., the deformation is further amplified and the material permanently collapses into a "black hole". Such reasoning also applies to nonlinear materials near the undeformed configuration. Orthotropic, and general anisotropic materials are substantially different from isotropic materials in terms of stability. In isotropic materials, no matter how large Young's modulus and no matter how close Poisson's ratio ν is to 0.5, it is always possible to find a sufficiently small timestep that keeps a dynamic simulation stable (albeit often with an accuracy loss due to locking as $\nu \to 0.5$). Anisotropic materials that are not positive-definite, however, are fundamentally unstable, under all timesteps and both under explicit or implicit integration. The same is true for (quasi-)static simulation. We shall see that this imposes restrictions on E_i, ν_{ij}, μ_{ij}.

Because $\mathcal{C}_{ortho}$ is block-diagonal, its positive-definiteness is equivalent to $\mu_{12} > 0, \mu_{23} > 0, \mu_{31} > 0$ plus positive-definiteness of the upper-left 3×3 block of $\mathcal{C}_{ortho}$. Using the Sylvester's theorem [35], this is equivalent to

$$E_1 > 0, \qquad E_2 > 0, \qquad E_3 > 0, \quad (18)$$

$$\nu_{12}\nu_{21} < 1, \quad \nu_{23}\nu_{32} < 1, \quad \nu_{31}\nu_{13} < 1, \quad \Upsilon > 0. \quad (19)$$

These restrictions can be easily derived by examining the upper-left 3×3 block of $\mathcal{S}_{ortho}$ [36].

Unlike the isotropic case where it is well-known that the Poisson's ratio ν has to be on the interval $(-1, 1/2)$, there is no analogous limits on ν_{ij} for orthotropic materials. In practice, it is very tedious to tune these parameters, as suboptimal values easily cause the simulation to explode, or introduce undue stiffness or other poor simulation behavior.

We demonstrate the shape of the stability regions in Fig. 1, for the naive choice where $\nu_{12}, \nu_{23}, \nu_{31}$ are made equal. The range of Young's modulus ratios which satisfies the positive-definiteness conditions (18) and (19) is limited to the regions shown in the figure. The stability region becomes smaller as ν_{ij} approaches 0.5. Such a simple choice of ν_{ij} greatly limits the range of stable Young's modulus ratios along the three material axes. Therefore, we propose a scheme to tune the orthotropic materials using the familiar intuition from the isotropic case. Our scheme provably

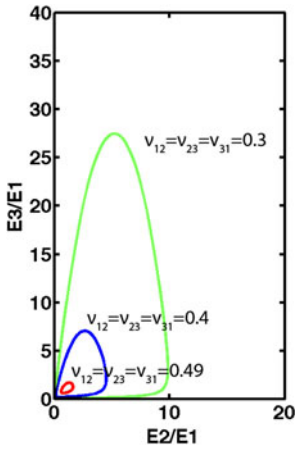

Fig. 1. **Stability of linear orthotropic materials.** The curves show the boundary of the stability region for the naive choice $\nu_{12} = \nu_{23} = \nu_{31}$; the other ν_{ij} are determined via (17).

guarantees positive-definiteness of the elasticity tensor. By applying (17) into (19), we obtain

$$\nu_{12}^2 < \frac{E_1}{E_2}, \qquad \nu_{23}^2 < \frac{E_2}{E_3}, \qquad \nu_{31}^2 < \frac{E_3}{E_1}. \tag{20}$$

Guided by the intuition from isotropic materials, we would like to use one parameter to simplify and control the assignments of all ν_{ij}. Equation (20) imposes upper and lower limits on all the three free ν_{ij} parameters. We control these three parameters using a single Poisson's ratio-like parameter ν as

$$\nu_{12} = \nu\sqrt{\frac{E_1}{E_2}}, \qquad \nu_{23} = \nu\sqrt{\frac{E_2}{E_3}}, \qquad \nu_{31} = \nu\sqrt{\frac{E_3}{E_1}}. \tag{21}$$

All three restrictions on ν_{ij} from (20) are satisfied by imposing $-1 < \nu < 1$. Using (17) and (21), we can express Υ as

$$\Upsilon = \frac{1}{(1+\nu)^2(1-2\nu)}. \tag{22}$$

To ensure $\Upsilon > 0$, we need to set $-1 \neq \nu < \frac{1}{2}$. Therefore, to ensure a positive-definite elasticity tensor $\mathcal{C}_{ortho}$,ν must satisfy the condition $-1 < \nu < \frac{1}{2}$. This is the familiar condition known with isotropic materials. Once ν has been selected, we can then use Equation (21) to safely determine all ν_{ij}. Fig. 2 demonstrates the volume-preservation effect of our linear orthotropic materials for three values of ν. For linear transversely isotropic materials, our formula simplifies to

$$\nu_{pz} = \nu_p\sqrt{\frac{E_p}{E_z}}. \tag{23}$$

In an orthotropic material, the shear moduli μ_{ij} are independent of E and ν. Suboptimal values of shear parameters, however, easily lead to excessive shear or stiff simulations that lock. It is useful to compute some reasonable μ_{ij} based only on Young's moduli and Poisson's ratios. Therefore, we

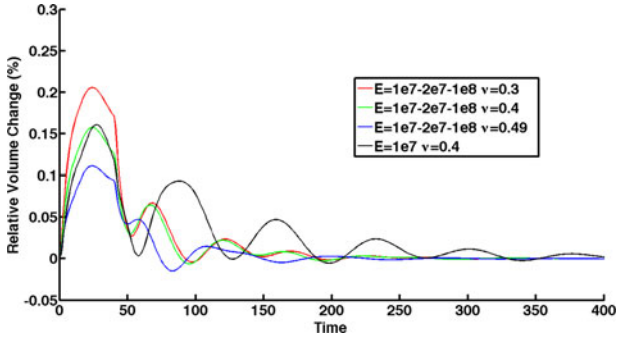

Fig. 2. **Controlling volume preservation with a single parameter** ν. Orthotropic dinosaur; stiffnesses are 1E7, 2E7, 1E8. Simulated under three Poisson's ratios $\nu = 0.3, 0.4, 0.49$. Isotropic material ($\nu = 0.4$) is shown black.

propose a scheme to set these values automatically. The shear modulus μ of a linear isotropic material is

$$\mu = \frac{E}{2(1+\nu)}. \tag{24}$$

We extend this equation to set μ_{ij} for linear orthotropic materials. Since we have found a parameter ν to control all ν_{ij} for linear orthotropic materials, we can use this parameter in (24). So an equation for a reasonable μ_{ij} is

$$\mu_{ij} = \frac{\overline{E}_{ij}}{2(1+\nu)}, \tag{25}$$

for some choice of a scalar $\overline{E}_{ij}$. There are several possible methods to assign $\overline{E}_{ij}$. For example, one can set $\overline{E}_{ij}$ to the maximum, minimum, arithmetic mean or geometric mean of E_i and E_j. Huber [37], followed by other researchers in mechanics [38], [39], used the geometric mean in predicting shear moduli of reinforced concrete slabs,

$$\mu_{ij} = \frac{\sqrt{E_i E_j}}{2(1+\sqrt{\nu_{ij}\nu_{ji}})}, \tag{26}$$

for $(i,j) = (1,2),(2,3),(3,1)$. Notice that if we use one parameter ν to control all Poisson's ratios, then $\sqrt{\nu_{ij}\nu_{ji}}$ is equal to ν and Huber's formula becomes an example of (25). We also examined other methods (max, min, arithmetic mean), and determined that the geometric mean offers good simulation properties (Fig. 3), especially when the three E_i differ by orders of magnitude. First, geometric mean is consistent with the other entries in the elasticity tensor $\mathcal{C}_{ortho}$. Applying (17) and (21) into (9) to (11) yields:

$$A = \frac{1}{(\nu+1)(1-2\nu)}\begin{bmatrix} E_1(1-\nu) & \sqrt{E_1E_2}\nu & \sqrt{E_1E_3}\nu \\ \sqrt{E_1E_2}\nu & E_2(1-\nu) & \sqrt{E_2E_3}\nu \\ \sqrt{E_1E_3}\nu & \sqrt{E_2E_3}\nu & E_3(1-\nu) \end{bmatrix}, \tag{27}$$

$$B = \frac{1}{1+\nu}\begin{bmatrix} \frac{\overline{E}_{12}}{2} & 0 & 0 \\ 0 & \frac{\overline{E}_{23}}{2} & 0 \\ 0 & 0 & \frac{\overline{E}_{31}}{2} \end{bmatrix}. \tag{28}$$

In the upper-left 3×3 block A of $\mathcal{C}_{ortho}$, non-diagonal entries contain a factor $\sqrt{E_iE_j}$. Using geometric mean to compute shear moduli is similar in spirit to this expression. Second,

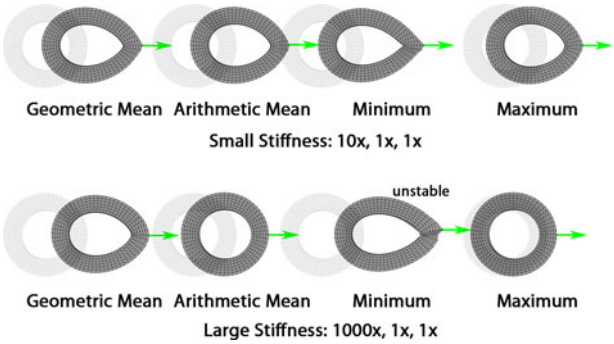

Fig. 3. **Setting the shear modulus for linear orthotropic materials.** The three stiffnesses are radial, longitudinal (in/out the paper), tangential. It can be seen that for small stiffness differences, each method produces acceptable results. For large stiffness differences, we also increased the force strength to generate large deformations. It can be seen that the geometric mean still bends the tube into an ellipse, which is correct given the low tangential stiffness and high radial stiffness. The other three methods cannot reproduce this effect.

geometric mean considers the magnitude of the Young's moduli in the two directions more evenly than arithmetic mean, especially when the values differ by orders of magnitude. For an orthotropic material where a material direction with a Young's modulus E_1 is several orders of magnitude stiffer than the other two directions, arithmetic mean would make $\overline{E}_{12}$ and $\overline{E}_{31}$ close to $\frac{E_1}{2}$, and therefore any difference between E_2 and E_3 is ignored for μ_{12} and μ_{31}. Using the geometric mean, however, produces a visible difference between μ_{12} and μ_{31} when E_2 and E_3 themselves differ substantially. In a transversely isotropic material, the shear modulus of the isotropic plane can be derived from E_p and ν_p like with isotropic materials, leaving μ_{zp} as the only free shear parameter. We can assign μ_{zp} as in Equation (25).

5 General Anisotropic Materials

We now extend the stability condition to general linear anisotropic materials. Such materials contain 21 independent entries and are given by a general symmetric elasticity tensor $\mathcal{C}$. Unlike orthotropic materials, general anisotropic materials couple shear and normal components: normal strains cause shear stresses and shear strains cause normal stresses. To simplify the tuning for them, we propose a subset of linear anisotropic materials that extend our stable linear orthotropic materials. These materials form a superset of our linear orthotropic materials and a proper subset of all linear anisotropic materials. We do so by modeling the elasticity tensor as

$$\mathcal{C}_{aniso} = \begin{bmatrix} A & C \\ C^T & B \end{bmatrix}, \tag{29}$$

where A is the same as in (27) and B is the same as in (28). The 3×3 matrix C couples shear and normal components,

$$C = \begin{bmatrix} \mathcal{C}_{14} & \mathcal{C}_{15} & \mathcal{C}_{16} \\ \mathcal{C}_{24} & \mathcal{C}_{25} & \mathcal{C}_{26} \\ \mathcal{C}_{34} & \mathcal{C}_{35} & \mathcal{C}_{36} \end{bmatrix}. \tag{30}$$

Note that matrix C is in general not symmetric. Each of the nine entries of C has an intuitive meaning: it controls the amount of shear stress in either 12, 23 and 31 plane resulting from a normal strain in either of the three material axes of orthotropicity. In the remainder of this section, we derive a necessary and sufficient condition on C to guarantee positive-definiteness of $\mathcal{C}_{aniso}$. We also propose simplified approaches to tune the nine entries of C and derive stability conditions for them.

We first observe that it is possible to factor out the effect of Young's moduli on stability. This makes it possible to freely alter E_1, E_2, E_3 without affecting simulation stability. Namely, Young's moduli E_1, E_2, E_3 can be factored out in (27) as

$$A = \hat{E}_A \tilde{A} \hat{E}_A, \quad \text{where} \tag{31}$$

$$\hat{E}_A = \begin{bmatrix} \sqrt{E_1} & 0 & 0 \\ 0 & \sqrt{E_2} & 0 \\ 0 & 0 & \sqrt{E_3} \end{bmatrix}, \quad \text{and} \tag{32}$$

$$\tilde{A} = \frac{1}{(\nu+1)(1-2\nu)} \begin{bmatrix} 1-\nu & \nu & \nu \\ \nu & 1-\nu & \nu \\ \nu & \nu & 1-\nu \end{bmatrix}. \tag{33}$$

If we choose to use the geometric mean in (28), we can factor Young's moduli from B as well:

$$B = \hat{E}_B \tilde{B} \hat{E}_B, \quad \text{where} \tag{34}$$

$$\hat{E}_B = \begin{bmatrix} (E_1E_2)^{\frac{1}{4}} & 0 & 0 \\ 0 & (E_2E_3)^{\frac{1}{4}} & 0 \\ 0 & 0 & (E_3E_1)^{\frac{1}{4}} \end{bmatrix}, \tag{35}$$

$$\text{and} \quad \tilde{B} = \frac{1}{2(1+\nu)} I. \tag{36}$$

Here, I is the 3×3 identity matrix. Equation (29) now becomes

$$\mathcal{C}_{aniso} = \hat{E} \widetilde{\mathcal{C}_{aniso}} \hat{E}, \quad \text{for} \tag{37}$$

$$\hat{E} = \begin{bmatrix} \hat{E}_A & 0 \\ 0 & \hat{E}_B \end{bmatrix}, \quad \widetilde{\mathcal{C}_{aniso}} = \begin{bmatrix} \tilde{A} & \tilde{C} \\ \tilde{C}^T & \tilde{B} \end{bmatrix}, \quad \text{for} \tag{38}$$

$$\tilde{C} = \hat{E}_A^{-1} C \hat{E}_B^{-1}. \tag{39}$$

Because $\hat{E}$ is a diagonal matrix, $\widetilde{\mathcal{C}_{aniso}}$ is symmetric. Because the entries of $\hat{E}$ are positive, $\mathcal{C}_{aniso}$ is positive-definite if and only if $\widetilde{\mathcal{C}_{aniso}}$ is positive-definite. Note that Young's moduli E_i no longer appear in $\widetilde{\mathcal{C}_{aniso}}$. We can therefore set the entries in $\tilde{C}$ independently of Young's moduli E_i. In this way, the values of Young's moduli will not affect the stability condition. This gives users the freedom to first tune $\widetilde{\mathcal{C}_{aniso}}$, and then arbitrarily tune E_i without compromising stability.

The next step is to find the conditions for positive-definiteness of $\widetilde{\mathcal{C}_{aniso}}$. By Schur's complement theorem [40], $\widetilde{\mathcal{C}_{aniso}}$ is positive-definite if and only if $\tilde{A}$ and its Schur's complement $\tilde{S} = \tilde{B} - \tilde{C}^T \tilde{A}^{-1} \tilde{C}$ are both positive definite. Using our stable orthotropic parameters, $\tilde{A}$ is always positive definite. So we need a condition on $\tilde{C}$ to ensure positive-definiteness of the symmetric matrix

$$\tilde{S} = \tilde{B} - \tilde{C}^T \tilde{A}^{-1} \tilde{C}. \tag{40}$$

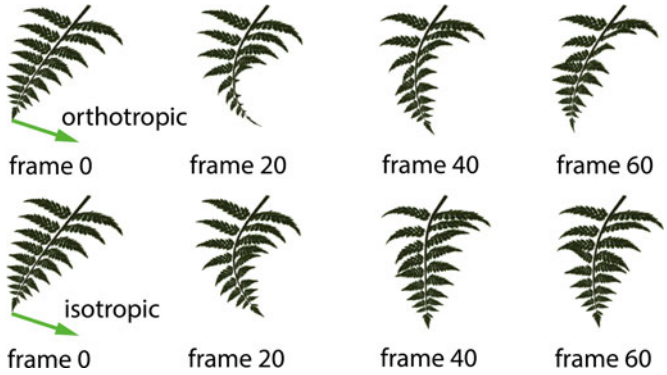

Fig. 4. **Orthotropic versus isotropic plant.** This orthotropic fern (top row) has stiffnesses that are 2×, 1×, and 0.01× higher than the isotropic fern (bottom row) in the longitudinal, transverse left-right and transverse up-down directions. We modeled the material axes to vary along the curved stem, so that they are always orthogonal to the stem. An interesting phenomenon can be observed at frames 20 and 40, similar to buckling: because the left-right direction is much stiffer than the up-down direction, the orthotropic fern's stem rotates (twists), causing most of the deformation to occur in the easiest material direction (up-down), which has now become aligned with the main deformation direction (left-right).

Because $\tilde{A}$ (and therefore $\tilde{A}^{-1}$) is positive-definite, matrix $\tilde{D} = \tilde{C}^T \tilde{A}^{-1} \tilde{C}$ is positive semidefinite: given any vector $y \in \mathbb{R}^3$, we have $y^T \tilde{D} y = (\tilde{C}y)^T \tilde{A}^{-1} (\tilde{C}y) \geq 0$. Because $\tilde{B}$ is a scaled identity matrix, S is therefore positive-definite if and only if all eigenvalues of $\tilde{D}$ are less or equal to $1/(2(1+\nu))$. Because $\tilde{D}$ is symmetric positive semidefinite, all its eigenvalues are greater or equal to zero, and its matrix 2-norm equals its largest eigenvalue. Therefore, the stability condition becomes

$$\|\tilde{D}\|_2 < \frac{1}{2(1+\nu)}. \tag{41}$$

We observe that matrix $\tilde{A}^{-1}$ has an easy-to-compute "square root", i.e., we can decompose $\tilde{A}^{-1}$ into $\tilde{A}^{-1} = L^T L = L^2$:

$$L = \frac{1}{3}\begin{bmatrix} p & q & q \\ q & p & q \\ q & q & p \end{bmatrix}, \quad \text{for} \tag{42}$$

$$p = \sqrt{1-2\nu} + 2\sqrt{1+\nu}, \; q = \sqrt{1-2\nu} - \sqrt{1+\nu}. \tag{43}$$

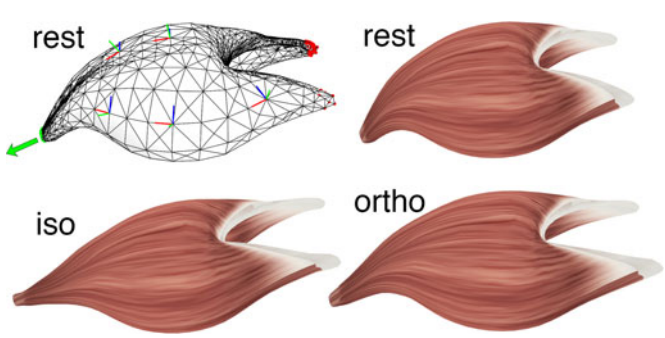

Fig. 5. **Stretched orthotropic muscle.** Red vertices are fixed, green vertices are constrained to a fixed displacement. Orthotropic stiffnesses in the up-down (green), transverse (blue) and longitudinal (red) directions are 1,000×, 30× and 1× higher than the isotropic stiffness, respectively. The orthotropic muscle preserves the original cross-section more, shrinks less near the attachment points and assumes a more organic shape. Top-left shows the simulation mesh and the spatially varying orthogonal directions.

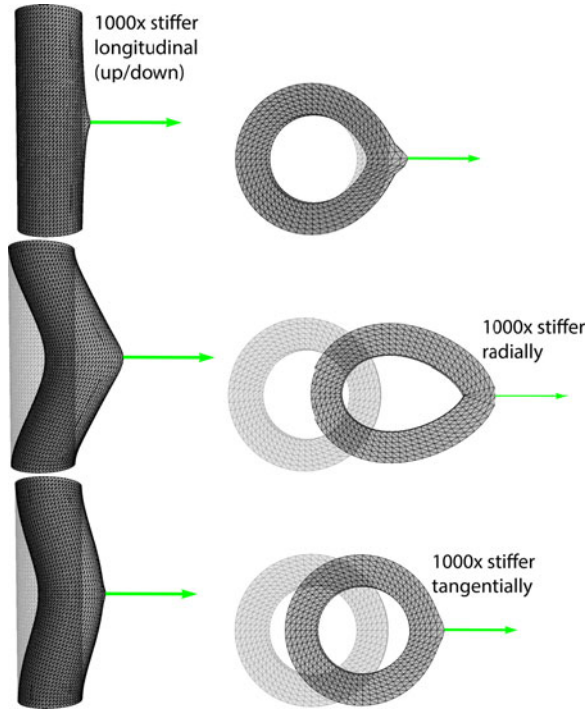

Fig. 6. Static poses for an orthotropic tube, (129,600 tets, 25,620 vertices), under a fixed force load. The right column gives the tube cross-section at the central height where the tube is being pulled. The local orthotropic axes vary across the object: for each element, they point along the longitudinal (up-down), radial and tangential directions. The rows have 1,000× higher Young's modulus in the longitudinal, radial and tangential tube direction, respectively. In the first row, high Young's modulus in the longitudinal direction prevents the tube from stretching up/down and therefore makes it harder for it to deform sideways. Note the local deformation in the horizontal direction. In the second row, the high radial Young's modulus preserves the thickness of the tube wall, as the tube cannot stretch radially. In the third row, high tangential Young's modulus makes it difficult to stretch the tube along its perimeter, i.e., preserves the perimeter length of the tube; note the radial local deformation.

Then, we can write

$$\tilde{D} = (L\tilde{C})^T (L\tilde{C}) = Y^T Y, \quad \text{for } Y = L\tilde{C}. \tag{44}$$

Note that Y is a general matrix (not necessarily symmetric). We now use the identity

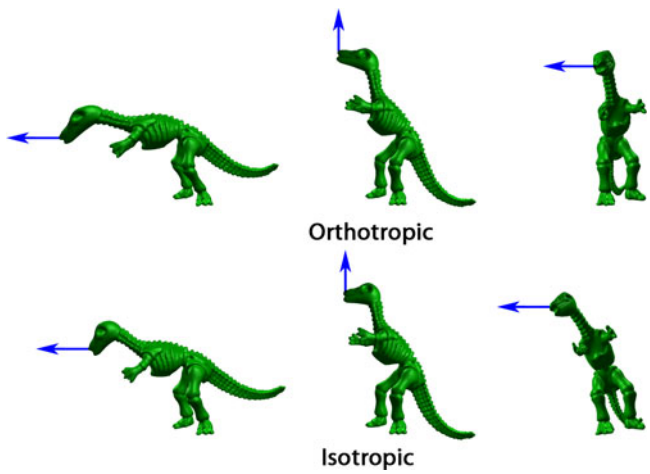

Fig. 7. **Orthotropic versus isotropic dinosaur.** The directions in the first, second and third column are 0.01×, 1× and 100× stiffer than the isotropic case.

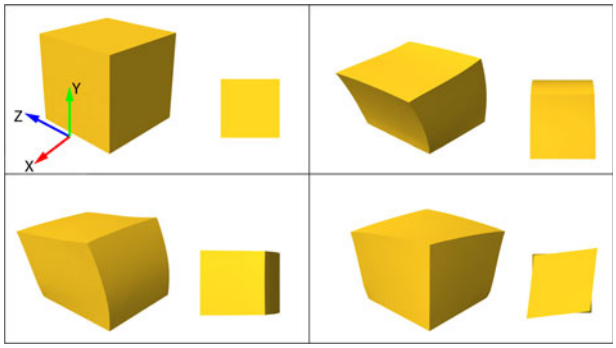

Fig. 8. **Non-orthotropic materials:** We added material anisotropy to this orthotropic cube, and loaded the cube with a constant uniform pressure in the negative y direction. In all cases, all entries of $\mathcal{C}$ were 0 except the denoted entry. Top-left: rest configuration. Top-right: Shear in the 12 plane, for $\mathcal{C}_{24} \neq 0$. Bottom-left: Shear in the 23 plane, for $\mathcal{C}_{25} \neq 0$. Bottom-right: Shear in the 31 plane, for $\mathcal{C}_{26} \neq 0$. The small image in each part shows the top view on the cube.

$$\|\tilde{D}\|_2 = \|Y\|_2^2 = \sigma_{max}(Y)^2, \tag{45}$$

where $\sigma_{max}(Y)$ is the largest singular value of Y. This can be seen as follows: for any matrix $Y, \|Y\|_2 = \sigma_{max}(Y)$ [41]. Let $Y = U\Sigma V^T$ be the singular value decomposition of Y, then we have

$$\|\tilde{D}\|_2 = \|Y^T Y\|_2 = \|V\Sigma^2 V^T\|_2 = \|\Sigma\|_2^2 = \sigma_{max}(Y)^2. \tag{46}$$

We can now state our final result: Tensor $\mathcal{C}_{aniso}$ is symmetric positive definite if and only if

$$\|Y\|_2 < \frac{1}{\sqrt{2(1+\nu)}}. \tag{47}$$

Users can tune our anisotropic materials by first tuning the orthotropic blocks A and B. When they want to add general (non-orthotropic) anisotropic effects, they can do so by setting the entries in $\tilde{C}$. Given a specific $\tilde{C}$, matrix $Y = L\tilde{C}$ is formed by computing L and multiplying it with $\tilde{C}$. Singular values of Y are then checked (Equation (47)) to inform the user whether the material is stable or not. Note that if the matrix $\tilde{C}$ is scaled by a scalar $\alpha \in \mathbb{R}, \|Y\|_2$ simply scales by α. This makes it possible to easily determine the largest $\alpha > 0$ such that $\tilde{C}$ is stable. In this way, the user gets an intuitive sense for how far along the specific anisotropic "direction" $\tilde{C}$ they can go before causing an instability.

Although each of the nine entries of $\tilde{C}$ has an intuitive meaning, it can be tedious to tune all nine entries of $\tilde{C}$ simultaneously. Instead, we consider two families of anisotropic materials. The first family consists of linear anisotropic materials where exactly one of the nine entries of $\tilde{C}$ is non-zero. This corresponds to adding an anisotropic effect of the material shearing in a chosen plane when subjected to a normal load in a chosen direction. If the value of the non-zero entry is $c \in \mathbb{R}$, stability condition (47) becomes

$$c < \frac{1}{\sqrt{2(1+\nu)}}. \tag{48}$$

We demonstrate this family of anisotropic materials in Fig. 8. Our stability condition (48) is experimentally tested

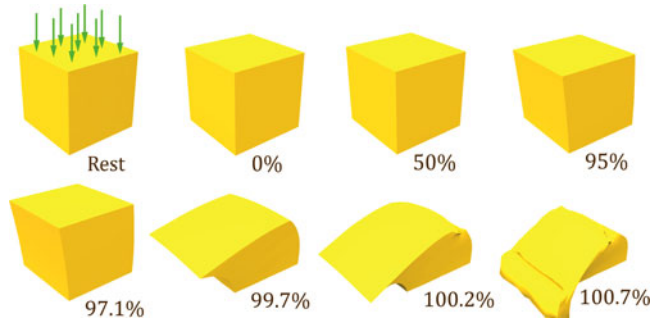

Fig. 9. **Stability of non-orthotropic materials:** We added the material anisotropy in the same way as in Fig. 8. We then computed the static equilibrium, under constant uniform pressure in the negative y direction, for several values of the anisotropic entry in C. A value of 0 percent denotes an orthotropic material ($C = 0$), and 100 percent denotes the stability limit from (48). As we cross the stability limit, the material becomes unstable.

in Fig. 9. It can be seen that the simulation becomes unstable when c reaches 100 percent of the stability threshold $1/\sqrt{2(1+\nu)}$.

The second family consists of Töplitz matrices $\tilde{C}$ defined as

$$\tilde{C} = \begin{bmatrix} \beta & \alpha & \gamma \\ \gamma & \beta & \alpha \\ \alpha & \gamma & \beta \end{bmatrix}, \tag{49}$$

where α, β, γ are scalar parameters. This matrix reduces the number of anisotropic parameters from nine to three. It gives symmetric anisotropic behavior along each of the three material orthotropic directions: for a given amount of normal strain in direction $i, i = 2, 3$, the resulting shear stress, and the entire geometric picture, is simply a rotated version of the situation for $i = 1$. For such a Töplitz matrix, the stability condition (47) can be easily simplified to

$$|\alpha + \beta + \gamma| < \frac{1}{\sqrt{2(1+\nu)(1-2\nu)}} \quad \text{AND} \tag{50}$$

$$\sqrt{(\alpha-\beta)^2 + (\beta-\gamma)^2 + (\gamma-\alpha)^2} < \frac{1}{1+\nu}. \tag{51}$$

We demonstrate stable anisotropic deformations from the Töplitz family in Fig. 10.

6 Results

We demonstrate orthotropic properties using a tube model (Fig. 6). We simulate an orthotropic plant (Fig. 4), muscle (Fig. 5), as well as a flexible dinosaur (Fig. 7). General anisotropic effects are demonstrated in Figs. 8, 9, and 10.

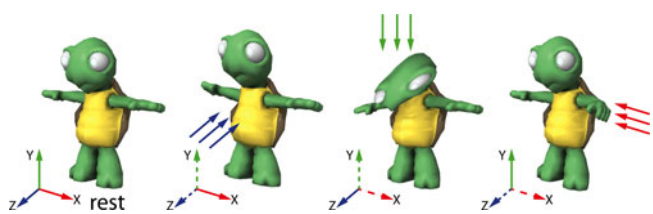

Fig. 10. **Non-orthotropic turtle deformed using a Töplitz matrix.** We used $\alpha = \beta = 0$ and $\gamma \neq 0$. We show the turtle deformed under static loads in the z, y and x direction, respectively. The two coordinate axes corresponding to the plane of the anisotropic shear are shown dashed.

TABLE 1
Timestep Computation Times and the Number of Employed Cores (#PSC = Number of Computing Cores for the Pardiso Solver, #IFC = Number of Computing Cores for Computing Internal Forces)

	vertices	tets	time	#PSC	#IFC
dinosaur	344	1,031	0.0060 sec	3	4
turtle	347	1,185	0.0043 sec	4	4
cube	2,980	9,382	0.049 sec	4	4
muscle	5,014	21,062	0.41 sec	8	12
tube	25,620	129,600	1.2 sec	12	12
fern	298,929	928,088	5.0 sec	12	8

Very small modifications are needed to the isotropic code. Runtime simulation times (Table 1) are unaffected, as we only need to change the computation of the elasticity tensor. This only affects the stiffness matrix computation, which is only done once at startup in a corotational linear FEM simulation. There is only a minor change in the stiffness matrix computation times. For example, the times to construct the isotropic and orthotropic global stiffness matrices were 1,993 and 2,038 msec, respectively (tube example).

7 Conclusion

We have augmented standard corotational linear FEM deformable simulations to support orthotropic and general anisotropic materials. We presented a complete modeling pipeline to simulate such materials, which requires minimal changes to existing simulators. We parameterized Poisson's ratios with a single parameter and therefore there are linear orthotropic materials that are not included in our one-dimensional family. For example, with isotropic stiffness ($E_1 = E_2 = E_3$), our one-dimensional family consists of isotropic materials, which excludes orthotropic materials with isotropic stiffness but distinct Poisson's ratios in the three orthogonal directions. Our stable anisotropic family does not include all the linear anisotropic materials. Our simulator is also limited to *linear* strain-stress relationships. We tune non-orthotropic anisotropic effects in the coordinate system of the three material orthotropic axes. In other coordinate systems, further transformations and more complex modeling would be required. We found that shearing is generally more present in anisotropic simulations than in isotropic simulations. Some anisotropic materials, such as those presented in Section 5, are designed to cause shear; and therefore these simulations exhibit large amounts of shear. We also observed substantial shearing in orthotropic simulations with large difference in Young's moduli along the three material axes ($1{,}000\times$ or more). In such cases, we found it advantageous to employ an anisotropic tetrahedral mesh, to better resolve shear. Structured tetrahedral meshes, such as those obtained by subdivision of voxels into tetrahedra, may "lock" and under-represent shears along certain coordinate directions. We would like to combine our method with inversion-preventing simulations [42], and investigate orthotropic and general anisotropic damping. A higher-level interface could be designed to allow users to edit anisotropic parameters in an intuitive or even goal-oriented way. Implementation of our stable orthotropic materials is available in Vega FEM 2.1, http://www.jernejbarbic.com/vega.

Acknowledgments

This research was sponsored in part by the National Science Foundation (CAREER-1055035, IIS-1422869), the Sloan Foundation, the Okawa Foundation, USC Annenberg Graduate Fellowship to Yijing Li, and a donation of two workstations by the Intel Corporation.

References

[1] M. Müller and M. Gross, "Interactive virtual materials," in *Proc. Graph. Interface*, 2004, pp. 239–246.
[2] A. F. Bower, *Applied Mechanics of Solids*. Boca Raton, FL, USA: CRC Press, 2011.
[3] J. Bonet and A. Burton, "A simple orthotropic, transversely isotropic hyperelastic constitutive equation for large strain computations," *Comput. Methods Appl. Mech. Eng.*, vol. 162, no. 1, pp. 151–164, 1998.
[4] G. Picinbono, H. Delingette, and N. Ayache, "Non-linear and anisotropic elastic soft tissue models for medical simulation," in Proc. *IEEE Int. Conf. Robot. Autom.*, 2001, vol. 2, pp. 1370–1375.
[5] R. T. Thije, R. Akkerman, and J. Huetink, "Large deformation simulation of anisotropic material using an updated lagrangian finite element method," *Comput. Methods Appl. Mech. Eng.*, vol. 196, no. 33, pp. 3141–3150, 2007.
[6] Y. Zhong, B. Shirinzadeh, G. Alici, and J. Smith, "A reaction-diffusion methodology for soft object simulation," in *Proc. ACM Int. Conf. Virtual Reality Continuum Its Appl.*, 2006, pp. 213–220.
[7] L. Kharevych, P. Mullen, H. Owhadi, and M. Desbrun, "Numerical coarsening of inhomogeneous elastic materials," *ACM Trans. Graph.*, vol. 28, no. 3, pp. 51:1–51:8, 2009.
[8] G. Picinbono, J.-C. Lombardo, H. Delingette, and N. Ayache, "Anisotropic elasticity and force extrapolation to improve realism of surgery simulation," in *Proc. IEEE Int. Conf. Robot. Autom.*, 2000, vol. 1, pp. 596–602.
[9] G. Picinbono, H. Delingette, and N. Ayache, "Non-linear anisotropic elasticity for Real-time surgery simulation," *Graphical Models*, vol. 65, no. 5, pp. 305–321, 2003.
[10] S.-H. Liao, R.-F. Tong, and J.-X. Dong, "Anisotropic finite element modeling for patient-specific mandible," *Comput. Methods Programs Biomed.*, vol. 88, no. 3, pp. 197–209, 2007.
[11] M. A. Sagar, D. Bullivant, G. D. Mallinson, and P. J. Hunter, "A virtual environment and model of the eye for surgical simulation," in *Proc. SIGGRAPH*, 1994, pp. 205–212.
[12] M. Sermesant, Y. Coudière, H. Delingette, N. Ayache, and J.-A. Désidéri, "An electro-mechanical model of the heart for cardiac image analysis," in *Proc. 4th Int. Conf. Med. Image Comput. Computer-Assisted Intervention*, 2001, pp. 224–231.
[13] M. Sermesant, H. Delingette, and N. Ayache, "An electromechanical model of the heart for image analysis and simulation," *IEEE Trans. Med. Imag.*, vol. 25, no. 5, pp. 612–625, May 2006.
[14] H. Talbot, S. Marchesseau, C. Duriez, M. Sermesant, S. Cotin, and H. Delingette, "Towards an interactive electromechanical model of the heart," *Interface focus*, vol. 3, no. 2, p. 20120091, 2013.
[15] O. Comas, Z. A. Taylor, J. Allard, S. Ourselin, S. Cotin, and J. Passenger, "Efficient nonlinear FEM for soft tissue modelling and its GPU implementation within the open source framework SOFA," in *Proc. 4th Int. Symp. Biomed. Simul.*, 2008, pp. 28–39.
[16] J. Teran, E. Sifakis, S. S. Blemker, V. Ng-Thow-Hing, C. Lau, and R. Fedkiw, "Creating and simulating skeletal muscle from the visible human data set," *IEEE Trans. Vis. Comput. Graph.*, vol. 11, no. 3, pp. 317–328, May 2005.
[17] E. Sifakis, I. Neverov, and R. Fedkiw, "Automatic determination of facial muscle activations from sparse motion capture marker data," *ACM Trans. Graph.*, vol. 24, no. 3, pp. 417–425, 2005.
[18] E. D. Sifakis, "Algorithmic aspects of the simulation and control of computer generated human anatomy models," Ph.D. dissertation, Stanford Univ., Stanford, CA, USA, 2007.
[19] X. Zhou and J. Lu, "Nurbs-based Galerkin method and application to skeletal muscle modeling," in *Proc. ACM Symp. Solid Phys. Model.*, 2005, pp. 71–78.
[20] G. Irving, J. Teran, and R. Fedkiw, "Invertible finite elements for robust simulation of large deformation," in *Proc. Symp. Comput. Animation*, 2004, pp. 131–140.

[21] N. Liu, X. He, Y. Ren, S. Li, and G. Wang, "Physical material editing with structure embedding for animated solid," in *Proc. Graph. Interface*, 2012, pp. 193–200.
[22] S. Martin, B. Thomaszewski, E. Grinspun, and M. Gross, "Example-based elastic materials," *ACM Trans. Graph.*, vol. 30, no. 4, pp. 72:1–72:8, 2011.
[23] F. Hernandez, G. Cirio, A. Perez, and M. Otaduy, "Anisotropic strain limiting," in *Proc. Congreso Español de Informática Gráfica*, 2013, vol. 2, pp. 1–7.
[24] P. Volino, N. Magnenat-Thalmann, F. Faure, et al., "A simple approach to nonlinear tensile stiffness for accurate cloth simulation," *ACM Trans. Graph.*, vol. 28, no. 4, pp. 105:1–105:16, 2009.
[25] O. Etzmuß, M. Keckeisen, and W. Straßer, "A fast finite element solution for cloth modelling," in *Proc. IEEE Pacific Conf. Comput. Graph. Appl.*, 2003, pp. 244–251.
[26] M. Huber, S. Pabst, and W. Straßer, "Wet cloth simulation," in *Proc. ACM SIGGRAPH Posters*, 2011, pp. 10.
[27] A. Garg, E. Grinspun, M. Wardetzky, and D. Zorin, "Cubic shells," in *Proc. Symp. Comput. Animation*, 2007, pp. 91–98.
[28] X. Peng and J. Cao, "A continuum Mechanics-based Non-orthogonal constitutive model for woven composite fabrics," *Composites Part A: Appl. Sci. Manuf.*, vol. 36, no. 6, pp. 859–874, 2005.
[29] B. Thomaszewski, S. Pabst, and W. Straßer, "Continuum-based strain limiting," *Comput. Graph. Forum*, vol. 28, no. 2, pp. 569–576, 2009.
[30] H. Wang, J. F. O'Brien, and R. Ramamoorthi, "Data-driven elastic models for cloth: Modeling and measurement," *ACM Trans. Graph.*, vol. 30, no. 4, p. 71, 2011.
[31] J. Allard, M. Marchal, S. Cotin, et al., "Fiber-based fracture model for simulating soft tissue tearing," *Med. Meets Virtual Reality*, vol. 17, pp. 13–18, 2009.
[32] W. Van Buskirk, S. Cowin, and R. N. Ward, "Ultrasonic measurement of orthotropic elastic constants of bovine femoral bone," *J. Biomech. Eng.*, vol. 103, no. 2, pp. 67–72, 1981.
[33] B. Lempriere, "Uniaxial loading of orthotropic materials." *AIAA J.*, vol. 6, no. 2, pp. 365–368, 1968.
[34] A. A. Shabana, *Theory of Vibration, Volume II: Discrete and Continuous Systems*. New York, NY, USA: Springer-Verlag, 1990.
[35] R. A. Horn and C. R. Johnson, *Matrix Analysis*. Cambridge, U.K.: Cambridge Univ. Press, 1985.
[36] B. Lempriere, "Poisson's ratio in orthotropic materials," *AIAA J.*, vol. 6, no. 11, pp. 2226–2227, 1968.
[37] M. Huber, "The theory of crosswise reinforced ferroconcrete slabs and its application to various important constructional problems involving rectangular slabs," *Der Bauingenieur*, vol. 4, no. 12, pp. 354–360, 1923.
[38] C. W. Bert, "Discussion: 'Theory of orthotropic and composite cylindrical shells, accurate and simple fourth-order governing equations'," *J. Appl. Mech.*, vol. 52, p. 982, 1985.
[39] S. Cheng and F. He, "Theory of orthotropic and composite cylindrical shells, accurate and simple Fourth-order governing equations," *J. Appl. Mech.*, vol. 51, pp. 736–744, 1984.
[40] Schur's Theorem [Online]. Available: en.wikipedia.org/wiki/Schur_complement, 2014.
[41] J. W. Demmel, *Applied Numerical Linear Algebra*. Philadelphia, PA, USA: SIAM, 1997.
[42] J. Teran, E. Sifakis, G. Irving, and R. Fedkiw, "Robust quasistatic finite elements and flesh simulation," in *Proc. Symp. Comput. Animation*, 2005, pp. 181–190.

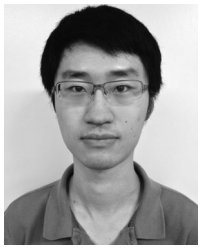

Yijing Li received the undergraduate degree from Tsinghua University in 2013. He is currently working toward the PhD degree in the Department of Computer Science, Viterbi School of Engineering, University of Southern California. His research interests include computer graphics and physically based animation. He is a member of the IEEE.

Jernej Barbič is an associate professor of computer science at USC. In 2011, MIT Technology Review named him one of the Top 35 Innovators under the age of 35 in the world (TR35). He published several papers on nonlinear solid deformation modeling, collision detection and contact, and interactive design of deformations and animations. He is an author of Vega FEM, an efficient free C/C++ software physics library for deformable object simulation. He is a member of the IEEE.